

An alternating finite difference material point method for numerical simulation of high explosive explosion problems

X. X. Cui¹, X. Zhang^{1,2}, K. Y. Sze³ and X. Zhou⁴

Abstract: Based on the material point method (MPM), an alternating finite difference material point (AFDMP) method is proposed for modeling the 3D high explosive (HE) explosion and its interaction with structures nearby. The initiatory detonation and eventual fluid structure interaction (FSI) are simulated by the standard MPM. On the other hand, the finite difference method (FDM) is employed to simulate the dispersion of the detonation products into the surrounding air where the particles degenerate to marker points which track the moving interface between detonation products and air. The conversion between MPM and FDM is implemented by the projection between the particles variables in MPM and the cell centers variables in FDM. In several numerical tests, predictions of the proposed method tests are in good agreement with theoretical solutions or empirical formulae. They illustrate that the method can yield good prediction for the entire HE explosion process.

Keywords: High explosive explosion, material point method, multi-material finite difference method, marker points, fluid-structure interaction

1 Introduction

The high explosive (HE) explosion consists of three different stages, namely the detonation through HE, the dispersion in which HE products disperse into the surrounding air, and fluid-structure interaction which excites the structures nearby. The whole process usually involves extreme deformation and multi-material interaction of different phases [Zukas and Walters (1998)]. Hence, the numerical simulation of the HE explosion is challenging. The Lagrangian finite element method

¹ School of Aerospace, Tsinghua University, Beijing 100084, China

² Corresponding author: xzhang@tsinghua.edu.cn

³ Department of Mechanical Engineering, The University of Hong Kong, Pokfulam, Hong Kong, China

⁴ Beijing Institute of Special Engineering Design and Research, Beijing 100028, China

(FEM), which has been used in various numerical analyzes, is capable of simulating history-dependent material and tracking the material interface. However, it suffers from mesh tangling which deteriorates its numerical accuracy and efficiency dramatically in simulating the dispersion. In contrast to Lagrangian method, Eulerian method such as FDM and finite volume method (FVM) employing fixed meshes is not plagued by mesh distortion but additional effort is needed to track the interface and the internal history variables. Youngs interface reconstruction method [Youngs (1982)] and level set method [Osher and Fedkiw (2001)] and fuzzy interface treatment [Ning and Chen (2004)] are commonly used to track the material interface. There are also some mixed methods which combine the advantages of Lagrangian and Eulerian descriptions and a well-known example is the arbitrary Lagrangian-Eulerian method (ALE) [Liu, Belytschko, and Chang (1986)]. The major numerical difficulty of ALE is developing an effective and efficient mesh moving scheme for complicated 3D problems. Furthermore, the numerical diffusion and dissipation still exist in ALE method. A detailed review on Lagrangian, Eulerian and their mixed methods was presented by Benson [Benson (1992)]. Recently, many meshless methods have been proposed as the alternatives for the traditional finite element and finite difference methods. Since their basic ideas are to discretize the material domain by a set of particles and construct the trial functions based on the particles without resorting to a mesh for interpolation, they have showed advantages over the mesh-based methods for problems associated with large deformation. Among them, the smoothed particle hydrodynamics (SPH) [Lucy (1977); Liu and Liu (2003)] and Material point method (MPM) [Sulsky, Chen, and Schreyer (1994); Sulsky, Zhou, and Schreyer (1995)] have been successfully applied to HE explosion problems. A comparison study of MPM and SPH in modeling hyper velocity impact problems was conducted by Ma et al. [Ma, Zhang, and Qiu (2009)]. By now, a lot of efforts have been devoted to study the effectiveness of various methods in solving HE explosion problems. The explosive is divided into two inhomogeneous parts by a very thin reaction zone. During the detonation, the explosive experiences large deformation. Therefore, meshless methods are widely used to simulate the detonation process as they can simulate the reaction of the HE in Lagrangian description yet they do not suffer from mesh distortion. Detonations of HE in air and underwater were simulated by SPH [Liu, Liu, Zong, and Lam (2003); Liu, Liu, Lam, and Zong (2003b)]. The numerical tests revealed the ability of the SPH in treating explosion problems of arbitrary charge shape and different orientations. Ma et al. [Ma, Zhang, Lian, and Zhou (2009)] proposed an adaptive material point method for simulating the HE explosion problems whilst Lian et al. [Lian, Zhang, Zhou, Ma, and Zhao (2011)] extended the MPM method to the explosively driven metal problems and the numerical results agreed well with the Gurney so-

lutions. Both studies illustrated MPM a powerful tool for studying detonation and other related explosive problems. In dispersion following detonation, the outward moving gaseous detonation products usually induces moving interfaces and strong shockwave. Thus, CFD (Computational Fluid Dynamics) methodologies based on Eulerian description are widely used. Ma et al. [Ma, Wang, and Ning (2008)] developed a multi-material Eulerian hydrodynamic code with modified Youngs' interface reconstruction algorithm for the simulations of explosion problems such as explosion in tunnel and steel shaped charge jet. Luccioni et al. [Luccioni, Ambrosini, and Danesi (2004)] employed AUTODYN to study the structural failure of a reinforced concrete building inflicted by an air blast load and the dispersion process of the HE products in air was simulated by the three-dimensional Euler FCT solver. Wu et al. [Wu and Hao (2005)] simulated the ground shock and air blast pressure generated from surface explosions using AUTODYN2D. When the shock wave reaches the structures nearby, structural damage may be induced via fluid-structure interaction (FSI). Methods based on Lagrangian framework are widely used for structural analyses because of their ability of modeling history-dependent materials. A common treatment is to discretize the structure by finite elements and the explosion effects are taken into account by applying the pressure load on the structure surface. For examples, a plate under air blast loading was studied by Jacinto et al. [Jacinto, Ambrosini, and Danesi (2001)] and the spallation in reinforced concrete plates subjected to blast loading was studied by Xu et al. [Xu and Lu (2006)]. Meshless methods based on Lagrangian framework are also widely used in these problems. Han et al. [Han, Liu, Rajendran, and Atluri (2006)] developed a three-dimensional dynamic numerical method based on the Meshless Local Petrov-Galerkin (MLPG) approach. Through several computational simulations, the method showed strong ability and efficiency for solving structural damage problems caused by high-speed contact and large deformations. Using MPM, Banerjee [Banerjee (2004)] simulated the fragmentation of cylinders due to explosively expanding gases generated by a high energy material inside the cylinders, and Hu et al. [Hu and Chen (2006)] studied the synergistic effects of blast and fragmentation on a concrete wall. Both studies concluded that the MPM possesses a great potential for simulating large deformation FSI problems at high strain-rate.

To simulate the HE explosion process and the relevant large deformation problems, much effort has been devoted to couple the afore-mentioned methods so as to tap the advantage of each method. Fairlie et al. [Fairlie and Bergeron (2002)] described a coupled methodology for simulating the surface-laid or buried charges explosions. In the methodology, the air and explosive are modeled in an Euler-FCT grid as a single ideal gas or in a multi-material Euler grid while the surrounding

soil and complex targets are modeled by Lagrangian grid. Zhang et al. [Zhang and Xu (2007)] investigated a cylindrical shell loaded by blast wave from a central charge. FVM is used to model the HE in ALE framework and FEM is adopted to model the shell in Lagrangian framework. Aktay et al. [Aktay and Johnson (2007)] developed a FEM/SPH coupling technique for high velocity impact (HVI) simulation of composite panels. In the technique, contact interfaces are employed to couple discrete smoothed particles and finite elements which are employed to model the parts undergoing large and small deformation, respectively. Guillkey et al. [Guillkey, Harman, and Banerjee (2007)] developed an approach for solving full-physics FSI problems using the Eulerian description (FVM) for fluids and the Lagrangian description (MPM) for solids. Zhang et al. [Zhang, Sze, and Ma (2006)] developed an explicit material point finite element method for HVI. In their method, the momentum equations are solved on a predefined regular grid for the severely deformed region and on FE mesh elsewhere. Lian et al. [Lian, Zhang, and Liu (2011)] developed a coupled approach in which the bodies with large and mild deformation are discretized by MPM and FEM, respectively. The interaction between two bodies is handled by contact method and the FE nodes on the contact interface are treated as special particles. To further improve the efficiency, Lian et al. [Lian, Zhang, and Liu (2012)] proposed an adaptive material point finite element method in which material domains are initially discretized into finite elements (FE). Depending on severity of the distortion or plastic strain being developed, some elements are adaptively converted into MPM particles. To simulate FSI problems with large deformations in the structure, Gilmanov et al. [Gilmanov and Acharya (2008)] developed an effective numerical method in which the hybrid immersed boundary method (HIBM) is employed to resolve complex boundaries for the fluid flow and MPM is coupled to resolve the structural stresses and deformation. The combined method is implemented in the framework of FDM.

Taking advantages of MPM and FDM, an alternating finite difference material point (AFDMP) method is developed in this paper to solve the HE explosion problems. MPM is employed in the detonation and the subsequent fluid FSI because of its sound ability for simulating history-dependent material and tracking the material interface in FSI problems with extreme deformation in the structure. To avoid the non-physical penetration at material interface between detonation products and the surrounding air, FDM but not MPM is introduced to simulate the dispersion. The particles are degenerated to marker points which only carry the position information for tracking the moving interface. The conversion between MPM and FDM is implemented by the projection between the particles variables in MPM and the cell centers variables in FDM. Hence, the process involved history-dependent materials and FSI problems are simulated by MPM and the process involved multi-material

fluid problems is simulated by FDM. The conversion between MPM and FDM is launched automatically by a user-specified criteria.

A TNT slab detonation and a shock tube are first studied to validate the AFDMP method. Afterward, 2D and 3D HE air explosion problems are simulated to illustrate the improvement of AFDMP over the standard MPM and FDM. Finally, the method is applied to a problem of HE air explosion and its interaction with a nearby steel plate. The numerical results are in good agreement with the theoretical results, experimental data or the predictions from the general commercial software AUTODYN. Comparing with afore-mentioned methods which solved HE explosion problems in Eulerian framework [Ning and Chen (2004); Ma, Wang, and Ning (2008)], AFDMP can treat material interface and complex FSI more effectively especially for 3D problems due to the employing of MPM. On the other hand, AFDMP is better than MPM in computational efficiency because the former saves the variables stored by particles for standard MPM.

The remaining part of this paper is organized as follows. Section 2 presents the governing equations under the Lagrangian and Eulerian descriptions. The material models employed in this paper are also introduced in this section. A brief description of MPM and FDM and their numerical implementations are presented in Section 3. Moreover, the scheme for treating multi-material fluid in FDM is proposed in detail. Several numerical examples are given in Section 4. Lastly, the conclusions are summarized in Section 5.

2 Governing equations and material models

The HE explosion can rapidly convert the original explosive charge into gaseous products at extremely high pressure that inflicts damages to the structures nearby. The whole process usually consists of the steady-state detonation through the HE, the dispersion of the detonation products to surrounding air and the interaction with the structures nearby. Since the primary materials and their properties are different in the three stages, different governing equations and material models are employed as follows.

2.1 Governing equations in updated Lagrangian description

During detonation and fluid-structure interaction, the history variables are important to describe the behavior of HE and the structure, respectively. Therefore, the updated Lagrangian description is employed for the continuum which is governed by the momentum balance equation [Hallquist (1998)]

$$\sigma_{i,j,j} + \rho f_i = \rho \ddot{u}_i \quad \forall x_i \in V \quad (1)$$

where V is the current material domain, σ_{ij} is the Cauchy stress, ρ is the current density, f_i is the body force density, \ddot{u} is the acceleration. The weak form of governing equation (1) can be obtained through weighted residuals as[Sulsky, Chen, and Schreyer (1994)]

$$\delta\Pi = \int_V \rho \ddot{u}_i \delta u_i dV + \int_V \sigma_{ij} \delta u_{i,j} dV - \int_V \rho f_i \delta u_i dV - \int_\Gamma t_i \delta u_i d\Gamma = 0 \tag{2}$$

where Γ is the boundary prescribed with traction t_i .

The mass conservation equation is

$$\dot{\rho} + \rho v_{i,j} = 0 \tag{3}$$

where v_i is the velocity and the energy equation is given by

$$\dot{E} = J\sigma_{ij}\dot{\epsilon}_{ij} = Js_{ij}\dot{\epsilon}_{ij} - Jp\dot{\epsilon}_{kk} \tag{4}$$

where J is the determinant of the deformation gradient matrix $F_{ij} = \partial x_i / \partial X_j$, E is the energy per unit initial volume. $\dot{\epsilon}_{ij}$ is the strain rate, $s_{ij} = \sigma_{ij} - p\delta_{ij}$ is the deviatoric stress and p represents the pressure. In AFDMP method, these governing equations will be solved by MPM schemes based on the same algorithms described in existing literature about MPM [Ma, Hanan, Komanduri, and Lu (2012)].

2.2 Governing equations in Eulerian description

The dispersion process of detonation products to the surrounding air is a multi-material fluid flow with moving material interfaces. Owing to the extremely high detonation and dispersion speeds, the explosion process is adiabatic. The detonation products and the surrounding air can be assumed to be inviscid and compressible. They can be described by the three-dimensional compressible Euler equations

$$\frac{\partial \mathbf{U}}{\partial t} + \frac{\partial \mathbf{f}}{\partial x} + \frac{\partial \mathbf{g}}{\partial y} + \frac{\partial \mathbf{h}}{\partial z} = 0 \quad t \geq 0, \quad (x,y) \in \mathbb{R}^3 \tag{5}$$

with suitable equation of state (EOS). In Eq. (5),

$$\mathbf{U} = \begin{pmatrix} \rho \\ \rho \dot{u}_1 \\ \rho \dot{u}_2 \\ \rho \dot{u}_3 \\ E \end{pmatrix}, \quad \mathbf{f} = \begin{pmatrix} \rho \dot{u}_1 \\ \rho \dot{u}_1^2 + p \\ \rho \dot{u}_1 \dot{u}_2 \\ \rho \dot{u}_1 \dot{u}_3 \\ (E + p)\dot{u}_1 \end{pmatrix}, \quad \mathbf{g} = \begin{pmatrix} \rho \dot{u}_2 \\ \rho \dot{u}_1 \dot{u}_2 \\ \rho \dot{u}_2^2 + p \\ \rho \dot{u}_2 \dot{u}_3 \\ (E + p)\dot{u}_2 \end{pmatrix}, \quad \mathbf{h} = \begin{pmatrix} \rho \dot{u}_3 \\ \rho \dot{u}_1 \dot{u}_3 \\ \rho \dot{u}_2 \dot{u}_3 \\ \rho \dot{u}_3^2 + p \\ (E + p)\dot{u}_3 \end{pmatrix} \tag{6}$$

where \dot{u}_1 , \dot{u}_2 and \dot{u}_3 are the velocity components along the x-, y- and z- directions, respectively; $E = \frac{1}{2}\rho(\dot{u}_1^2 + \dot{u}_2^2 + \dot{u}_3^2) + \rho e$ is total energy per unit volume; e is internal specific energy and pressure p can be obtained from an EOS. These conservation laws will be solved by FDM schemes in AFDMP method.

2.3 Material models

2.3.1 High explosive model

During the detonation process, the reactive wave propagates at very high speed inside the HE [Zukas and Walters (1998)]. The exothermic reaction is completed within a few microseconds with the HE completely converted to gaseous products. Most of the earlier works use the “artificial detonation model” [Liu and Liu (2003)] which considers the explosive as a group of gaseous products with the same energy and volume of the initial explosive charge. In this paper, we use the “real detonation model” [Liu and Liu (2003)] which lights the explosive according to the reactive wave’s propagation. Comparison of the results yielded by the two detonation models are presented in Section 4.1.

In the initialization phase, a lighting time t_L is calculated for each particle (MPM) by dividing the distance from the detonation point by the detonation speed. After the detonation, the gaseous products are controlled by the EOS. The real pressure p of the gaseous products is determined by multiplying the pressure p_{EOS} obtained from EOS with a burn fraction F that controls the release of chemical energy [Hallquist (1998)], namely

$$p = F \cdot p_{EOS} \quad (7)$$

$$F = \begin{cases} \frac{(t-t_L)D}{1.5h} & t > t_L \\ 0 & t < t_L \end{cases} \quad (8)$$

where h is the characteristic size of a particle and t denotes the current time. Several time steps are often required for F to attain or exceed unity. Once it is done, F is set to and kept at unity. Using this method, the discontinuous detonation wave is smoothed and assumes a continuous but rapidly changing wavefront.

After detonation, the gaseous products are described by an EOS. In this paper, the following Jones-Wilkins-Lee(JWL) equation is used

$$p = A\left(1 - \frac{\omega}{R_1 V}\right)e^{-R_1 V} + B\left(1 - \frac{\omega}{R_2 V}\right)e^{-R_2 V} + \frac{\omega E_0}{V} \quad (9)$$

Moreover, TNT with density 1630 kg/m^3 and detonation speed of 6930 m/s are used in the simulation as the HE. The parameters of JWL EOS are taken from [Liu, Liu, Lam, and Zong (2003a)] as $A = 3.712 \times 10^{11} \text{ N/m}^2$, $B = 3.21 \times 10^9 \text{ N/m}^2$, $R_1 = 4.15$, $R_2 = 0.95$, $\omega = 0.3$, energy per initial volume $E_0 = 6993 \times 10^6 \text{ J/m}^3$. Moreover, this EOS is combined with the null material model in which the material strength is ignored.

2.3.2 Air model

Similar to the gaseous products of HE, air is modeled as a null material model with EOS. Here, the ideal gas EOS is used, i.e.

$$p = (\gamma - 1)\rho e = (\gamma - 1)\left[E - \frac{1}{2}\rho(u^2 + v^2 + w^2)\right] \quad (10)$$

where $\rho = 1.225 \text{ kg/m}^3$ and $e = 2.0685 \times 10^5 \text{ J/kg}$.

2.3.3 Steel model

The simplified Johnson-Cook material model [Johnson and Cook (1983)] is employed in the last numerical example to describe the property of a steel plate. The model accounts for the strain rate effect and has widely used to model the behavior of metal during impact and explosion. The yield stress is given by

$$\sigma_y = (A + B\varepsilon^n)(1 + C \ln \dot{\varepsilon}^*) \quad (11)$$

where ε is the equivalent plastic strain, $\dot{\varepsilon}^* = \dot{\varepsilon}/\dot{\varepsilon}_0$ is the dimensionless plastic strain rate with $\dot{\varepsilon}_0 = 1 \text{ s}^{-1}$. The material constants are taken to be $A = 350 \text{ MPa}$, $B = 275 \text{ MPa}$, $n = 0.36$ and $C = 0.022$.

The pressure of steel is updated by the Mie-Grüneisen EOS as

$$p = p_H \left(1 - \frac{\gamma\mu}{2}\right) + \gamma\rho E \quad (12)$$

where

$$p_H = \begin{cases} \rho_0 C_0^2 [\mu + (2S - 1)\mu^2 + (S - 1)(3S - 1)\mu^3] & \mu > 0 \\ \rho_0 C_0^2 \mu & \mu < 0 \end{cases} \quad (13)$$

In Eqs. 12 and 13, the subscript H refers to the Hugoniot curve and $\mu = \rho/\rho_0 - 1$ is used to represent the compression of solid with ρ_0 being the stress-free solid density. Moreover, γ , C_0 and S are the material constants which are taken as $\gamma = 2.17$, $C_0 = 4569 \text{ m/s}$ and $S = 1.49$ for the last numerical example. The material constants of the Simplified Johnson-Cook model used in this paper is taken from the material model "STEEL 1006" in AUTODYN.

3 Alternating finite difference material point (AFDMP) method

In the problem shown in Fig.1, a HE charge is burned into the gaseous products which disperse to the surrounding air and then interact with the structure. The whole region can be divided into the fluid and interaction regions separated by the

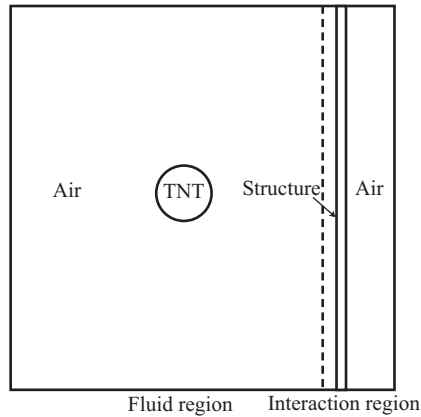


Figure 1: A typical HE explosion problem

dash line. The whole process of the HE explosion can be divided into three stages. At the beginning of the simulation, the fluid region is activated while the interaction region remains intact. The HE and air are discretized by particles. MPM is employed for the detonation so that the “real detonation model” and burn fractions can be applied to every HE particles to track the history variables. After the detonation is over, the variables are mapped to the cell-center points of the background grid and then the traditional FDM is employed to simulate the dispersion. The particles in the fluid region are degenerated to massless marker points to track the moving interface. When the pressure of cell-center points near the boundary, i.e. the dash line in Fig.1, attains a prescribed value, arrival of the shock wave front is assumed and the interaction region would be activated. The interaction process is simulated by MPM so that the history variables of structure can be recorded to characterize the material damage.

The detailed schemes for the three stage are presented in the following three subsections. The treatment for material interface are provided in Section 3.4.

3.1 Stage 1: MPM for detonation process

As a pre-processing step, we define the background grid in the fluid region, and discretize the material region by particles, see Fig.2. MPM is employed to simulate the detonation until all the HE particles have been burned. MPM is an extension of the FLIP particle in cell (PIC) method [Brackbill and Ruppel (1986)] in computational fluid dynamics to the computational solid mechanics. In MPM, all the material variables are carried by the particles including mass, position, velocity,

strain, stress, etc. In each time step, the particles are rigidly attached to the background grid in which the momentum equation is solved with the framework of the standard finite element method. The variables in background grid are obtained by mapping the variables from particles to the grid nodes. Then, the positions and velocities of particles are updated by mapping back the kinematic solution of the grid nodes. Afterward, the deformed grid is discarded and a new regular grid is used in the next time step. Thus, complications associated with mesh distortion are avoided. In general, a fixed regular grid can be used for all time steps. Since the ma-

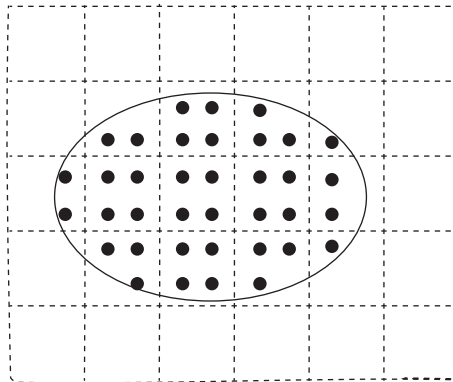


Figure 2: Material point discretization

terial domain is discretized with a set of particles, the density can be approximated as

$$\rho(\mathbf{x}) = \sum_{p=1}^{n_p} m_p \delta(\mathbf{x} - \mathbf{x}_p) \tag{14}$$

where n_p denotes the total number of particles; δ is Dirac Delta; m_p is the mass and \mathbf{x}_p is the position of particle p . Since the mass is carried by the particles, the mass conservation is automatically satisfied in MPM. Substituting (14) into the weak form 512 leads to

$$\sum_{p=1}^{n_p} m_p \ddot{u}_{ip} \delta u_{ip} + \sum_{p=1}^{n_p} m_p \delta u_{ip,j} - \sum_{p=1}^{n_p} m_p f_{ip} \delta u_{ip} - \sum_{p=1}^{n_p} \frac{m_p}{\rho_p} t_i h^{-1} \delta u_{ip} = 0 \tag{15}$$

where h denotes the thickness of the boundary layer.

Since the particles are rigidly attached to the computational grid, the displacement of particle p , \mathbf{u}_p , can be obtained by mapping from their grid node values \mathbf{u}_I using

the standard finite element interpolation functions of the grid as

$$\mathbf{u}_p = \sum_{I=1}^{n_g} N_{Ip} \mathbf{u}_{Ip} \quad (16)$$

where $N_{Ip} = N_I(\mathbf{x}_p)$ is the interpolation function of grid node I evaluated at the position of particle p . In this paper, the 8-node hexahedron interpolation is used and the function is given by

$$N_{Ip} = \frac{1}{8} (1 + \xi_p \xi_I) (1 + \eta_p \eta_I) (1 + \zeta_p \zeta_I) \quad I = 1, 2, \dots, 8 \quad (17)$$

where (ξ_I, η_I, ζ_I) take their nodal value of ± 1 on grid node I and (ξ_p, η_p, ζ_p) denote the natural coordinates of particle p . If the particle is outside the hexahedron, $N_{Ip} = 0$.

The detailed implementation of MPM for detonation process in a time step (from n to $n + 1$) can be summarized as follows.

(1) Map the mass m and momentum p of all MPM particles to the background grid by

$$m_I^n = \sum_{p=1}^{n_p} N_{Ip}^n m_p \quad (18)$$

$$p_{il}^n = \sum_{p=1}^{n_p} m_p N_{Ip}^n v_{ip}^n \quad (19)$$

to obtain the mass and momentum of grid nodes.

(2) Compute the grid nodal internal force f^{int} and external force f^{ext} by

$$f_{il}^{\text{int},n} = - \sum_{p=1}^{n_p} \nabla N_{Ip}^n \cdot \boldsymbol{\sigma}_{ijp} \frac{m_p}{\rho_p} \quad (20)$$

$$f_{il}^{\text{ext},n} = \sum_{p=1}^{n_p} m_p N_{Ip}^n f_{ip}^n + \sum_{p=1}^{n_p} N_{Ip}^n h^{-1} t_{ip}^n \frac{m_p}{\rho_p} \quad (21)$$

(3) Integrate the momentum equation by

$$p_{il}^{n+1} = p_{il}^{n+1} + f_{il}^n \Delta t^n \quad (22)$$

where

$$f_{il}^n = f_{il}^{\text{int},n} + f_{il}^{\text{ext},n} \quad (23)$$

(4) Update the velocity and position of particles by mapping their increments back to particles as

$$x_{ip}^{n+1} = x_{ip}^n + \sum_{l=1}^8 \frac{p_{il}^{n+1}}{m_l^n} N_{lp}^n f_{ip}^n \Delta t^n \quad (24)$$

$$v_{ip}^{n+1} = v_{ip}^n + \sum_{l=1}^8 \frac{f_{il}^n}{m_l^n} N_{lp}^n \Delta t^n \quad (25)$$

(5) Map the velocity back to the grid nodes

$$v_{il}^{n+1} = \frac{\sum_{p=1}^{n_p} m_p N_{lp}^n v_{ip}^n}{m_l^k} \quad (26)$$

(6) The incremental strain and spin tensors are calculated by

$$\Delta \epsilon_{ijp}^n = \frac{1}{2} \sum_{l=1}^8 (N_{lp,j}^{n+1} v_{il}^{n+1} + N_{lp,i}^{n+1} v_{jl}^{n+1}) \Delta t^n \quad (27)$$

$$\Delta \Omega_{ijp}^n = \frac{1}{2} \sum_{l=1}^8 (N_{lp,j}^{n+1} v_{il}^{n+1} - N_{lp,i}^{n+1} v_{jl}^{n+1}) \Delta t^n \quad (28)$$

(7) Update the density of particles as

$$\rho_p^{n+1} = \rho_p^n / (1 + \Delta \epsilon_{ijp}^n) \quad (29)$$

(8) For Newtonian fluid, the $\Delta \Omega_{ijp}^n$ is ignored, hence the stress of particles is updated by

$$\sigma_{ijp}^{n+1} = \sigma_{ijp}^n + \Delta \sigma_{ijp}^n \quad (30)$$

where $\Delta \sigma_{ijp}^n$ is calculated by the EOS described in Section 2.3.

(9) All the history information has been updated and stored in particles. The current time step ends after we discard the deformed background grid and employ a new regular grid for next time step.

3.2 Stage 2: FDM for dispersion process

As described in section 2.3, the real pressure p of the gaseous products is obtained by multiplying the pressure p_{EOS} calculated from an EOS with a burn fractions F that controls the release of chemical energy in the detonation. After $F \geq 1$, the HE particles are considered to be fully burned and the detonation ends when all

HE particles have been fully burned. Then, the conversion from MPM to FDM is carried out to obtain the initial variables of the cell-center points and FDM is employed to solve the conservation laws described in Section 2.2.

The detailed implementation begins with the conversion from MPM to FDM. The conversion must secure the conservations of mass, momentum and energy. In the following, the cell k in Fig.3 is taken as an example. After the conversion criterion

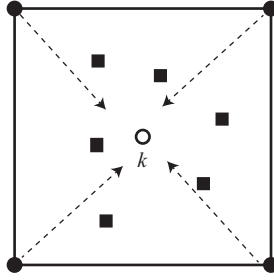


Figure 3: Conversion sketch in cell k (solid squares are particles, solid circles are background grid nodes and the hollow circle denotes the cell-center point employed in FDM)

is satisfied at time step n , we map the mass and momentum from background grid nodes to cell-center point k via the shape function, namely

$$m_c^n = \sum_{I=1}^8 m_I^n N_{Ic}^n \quad (31)$$

$$p_{ic}^n = \sum_{I=1}^8 p_{iI}^n N_{Ic}^n \quad (32)$$

where m_c^n and p_{ic}^n denote the mass and momentum of the center point of the cell c in time step n . The internal energy of cell-center point k , $e_c^{\text{int},n}$, is calculated by adding all the particles' internal energy in the cell as

$$e_c^{\text{int},n} = \sum_{p=1}^{n_p} e_p^{\text{int},n} \quad (33)$$

Finally, the conserved variables of the cell-center point k in FDM can be obtained by

$$\rho_c^n = \frac{m_c^n}{V_c} \quad (34)$$

$$(\rho v)_{ic}^n = \rho_c^n \frac{p_{ic}^n}{m_c^n} \tag{35}$$

$$E_c^n = \frac{e_c^{\text{int},n} + \frac{1}{2} m_c^n \left(\frac{p_{ic}^n}{m_c^n}\right)^2}{V_c} \tag{36}$$

where V_c is the volume of cell k . Up to this point, all conserved variables of the cell-center points for FDM have been obtained from MPM. Next, the particles for MPM are degenerated to the massless marker points which only carry the position information for tracking the material interface.

After the conversion, all variables of the fluid are carried by the cell-center points which are defined by the regular background cells in MPM as shown in Fig.4. On the other hand, the marker points converted from the particles are used to track the material interface. To simulate the dispersion of the detonation products to the surrounding air, FDM is employed to solve the governing equations (5) in Section 2.2 which can readily extend to three-dimensional problems by fractional steps method[Yanenko (1971)]. The method implemented here is a explicit three-dimensional finite difference scheme. Its implementation in a time step (from n to $n + 1$) can be summarized as follows.

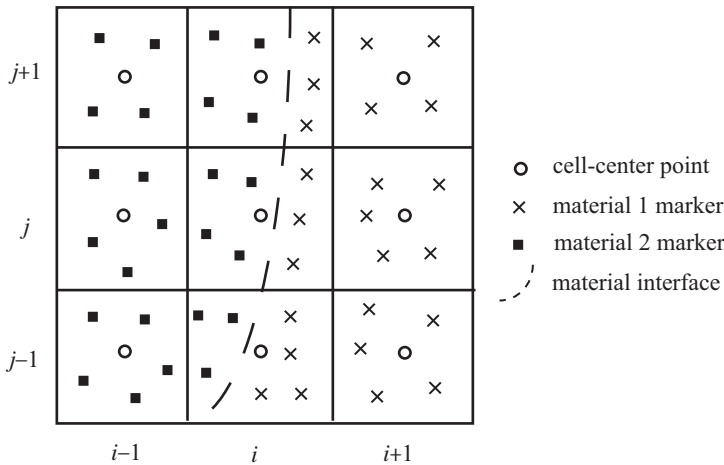


Figure 4: Finite difference discretization

(1) Since the fluid region contains both air and HE products, we begin with marking the cell type using the marker points. The cells containing marker points of both air and HE products are defined as mixed cells. The remaining cells are pure cells.

(2) For pure cells, the pressure of HE products and air are obtained by Eq.(9) and Eq.(10), respectively. For mixed cells, a group of equations to be presented in Section (3.4) would be solved to determine the equilibration pressure.

(3) To avoid the non-physical oscillations near the shockwave, take x direction as an example, adaptive artificial viscosity [Zhang (2010)] is used which introduce an adaptive artificial viscosity into the conservation variable U_i^n , namely

$$\bar{U}_i^n = U_i^n + \frac{1}{2} \eta \theta_i^n (U_{i+1}^n - 2U_i^n + U_{i-1}^n) \quad (37)$$

$$\theta_i^n = \left| \frac{|\rho_{i+1}^n - \rho_i^n| - |\rho_i^n - \rho_{i-1}^n|}{|\rho_{i+1}^n - \rho_i^n| + |\rho_i^n - \rho_{i-1}^n|} \right| \quad (38)$$

where η is a parameter to be adjusted empirically to meet the requirements for different problems or determined according to the time step Δt , spatial step Δx and sound speed c as

$$\eta = \frac{\Delta t \cdot c}{\Delta x} \left(1 - \frac{\Delta t \cdot c}{\Delta x}\right) \quad (39)$$

(4) The fractional steps method [Yanenko (1971)] is introduced to split the three-dimensional problem to three one-dimensional nonviscous flow problems. To reduce the artificial affect introduced by the integration sequence, the splitting can be implemented as

$$\mathbf{U}^{n+1} = L_z\left(\frac{1}{2}\Delta t\right)L_y\left(\frac{1}{2}\Delta t\right)L_x\left(\frac{1}{2}\Delta t\right)L_x\left(\frac{1}{2}\Delta t\right)L_y\left(\frac{1}{2}\Delta t\right)L_z\left(\frac{1}{2}\Delta t\right)\mathbf{U}^n \quad (40)$$

where $L_x(\Delta t)$, $L_y(\Delta t)$ and $L_z(\Delta t)$ are the difference operators of Eq.(5) in x , y and z direction, respectively; \mathbf{U}^n are the conservation variables \bar{U}_i^n defined in Eq.(37). In this paper, a second order Lax-Wendroff [Lax and Wendroff (1964)] finite difference scheme is employed for each direction, $L_x(\Delta t)$, $L_y(\Delta t)$ and $L_z(\Delta t)$ are advanced as

$$\begin{aligned} L_x(\Delta t)\mathbf{U}_i^n = & \mathbf{U}_i^n - \frac{1}{2} \frac{\Delta t}{\Delta x} [\mathbf{f}(\mathbf{U}_{i+1}^n) - \mathbf{f}(\mathbf{U}_{i-1}^n)] \\ & + \frac{1}{2} \left(\frac{\Delta t}{\Delta x}\right)^2 [\mathbf{f}(\mathbf{U}_{i+1}^n) - 2\mathbf{f}(\mathbf{U}_i^n) + \mathbf{f}(\mathbf{U}_{i-1}^n)] \end{aligned} \quad (41)$$

$$\begin{aligned} L_y(\Delta t)\mathbf{U}_j^n = & \mathbf{U}_j^n - \frac{1}{2} \frac{\Delta t}{\Delta x} [\mathbf{g}(\mathbf{U}_{j+1}^n) - \mathbf{g}(\mathbf{U}_{j-1}^n)] \\ & + \frac{1}{2} \left(\frac{\Delta t}{\Delta x}\right)^2 [\mathbf{g}(\mathbf{U}_{j+1}^n) - 2\mathbf{g}(\mathbf{U}_j^n) + \mathbf{g}(\mathbf{U}_{j-1}^n)] \end{aligned} \quad (42)$$

$$L_z(\Delta t)\mathbf{U}_k^n = \mathbf{U}_i^n - \frac{1}{2} \frac{\Delta t}{\Delta x} [\mathbf{h}(\mathbf{U}_{k+1}^n) - \mathbf{h}(\mathbf{U}_{k-1}^n)] + \frac{1}{2} \left(\frac{\Delta t}{\Delta x}\right)^2 [\mathbf{h}(\mathbf{U}_{k+1}^n) - 2\mathbf{h}(\mathbf{U}_k^n) + \mathbf{h}(\mathbf{U}_{k-1}^n)] \tag{43}$$

(5) To track the interface of the multi-material fluid and compute the volume fraction of the mixed cells, the position of marker points \mathbf{X}_m are updated by the velocity field. Taking the 2-dimensional region shown in Fig.5 as an example. It is discretized into 9 cells with “o” denoting the cell-center points. Consider a marker point $m(x, y)$ in cell (i, j) with coordinates $(x_{i,c}, y_{j,c})$. The following normalized coordinates are defined for $m(x, y)$

$$\xi_x = \frac{x - x_{i,c}}{\Delta x}, \quad \xi_y = \frac{y - y_{j,c}}{\Delta x} \tag{44}$$

The velocity $\mathbf{v}_m^n(x, y)$ of $m(x, y)$ can be calculated by the polynomial interpolation using those of the 9 (27 for 3-dimensions) cell-center points in and around cell (i, j) as

$$\mathbf{v}_m^n(x, y) = f(\mathbf{v}_m^n(x_{i-1,c}, y), \mathbf{v}_m^n(x_{i,c}, y), \mathbf{v}_m^n(x_{i+1,c}, y), \xi_x) \tag{45}$$

where

$$f(\mathbf{v}_1, \mathbf{v}_2, \mathbf{v}_3, \xi) = \frac{\mathbf{v}_1 - 2\mathbf{v}_2 + \mathbf{v}_3}{2} \xi^2 + \frac{\mathbf{v}_3 - \mathbf{v}_2}{2} \xi + \mathbf{v}_2 \tag{46}$$

is the interpolating function obtained by the quadratic polynomial in each direction. Now, $\mathbf{v}_m^n(x_{r,c}, y)$ being the velocity of the spatial point with x-coordinate of the cell-center point (r, j) and y-coordinate of the marker point $m(x, y)$ is

$$\mathbf{v}_m^n(x_{r,c}, y) = f(\mathbf{v}_{r(j-1),c}^n, \mathbf{v}_{r,j,c}^n, \mathbf{v}_{r(j+1),c}^n, \xi_y) \quad r = i - 1, i, i + 1; \tag{47}$$

in which $\mathbf{v}_{r,s,c}^n$ is the velocity of the cell-center point (r, s) .

The position of the marker point $m(x, y)$ in next time step is updated by

$$\mathbf{X}_m^{n+1} = \mathbf{X}_m^n + \mathbf{v}_m^n(x, y)\Delta t^n \tag{48}$$

This completes one time step of the explicit FDM scheme for simulating the dispersion process.

3.3 Stage 3: MPM for interaction process

The conversion from FDM to MPM is carried out when the pressure of cell-center points near the boundary between the two regions reaches an user-specified value

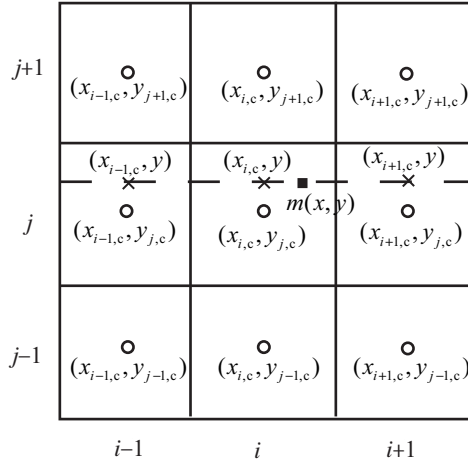


Figure 5: Updating position of marker points

which is set to be 1.0×10^{-5} MPa for the numerical examples in Sections (4.3) and (4.5). There are three different cases for various cell types and regions as follows.

(1) For the pure cell which has marker points of only one material, we discard the marker point and redistribute its variables to 8 material particles as if we initialize MPM. The particle variables are set by those of cell-center points obtained by FDM in Stage 2 as

$$m_p^n = \frac{1}{8} \rho_c^n V_c \tag{49}$$

$$v_{ip}^n = \frac{(\rho v)_{ic}^n}{\rho_c^n} \tag{50}$$

$$e_p^{\text{int},n} = \frac{1}{8} e_c^{\text{int},n} \tag{51}$$

$$\sigma_p^n = -p_c^n \tag{52}$$

where p_c^n is the pressure of the cell-center points, and

$$x_{ip}^n = x_{ic} \pm 0.25 \Delta x_i \tag{53}$$

where Δx_i denotes Δx , Δy or Δz in different directions.

(2) For the mixed cell which has marker points of both air and HE products, the particles are converted from the marker points at the same position. The variables of the cell-center points are divided into two parts for different materials which were

calculated in Stage 2. Then, the mass and internal energy of different materials are distributed to the particles associated with the respective materials as

$$m_{rp}^n = \frac{\rho_{rc}^n \theta_r V_c^n}{n_{br}} \tag{54}$$

$$e_{rp}^{\text{int},n} = \frac{e_{rc}^{\text{int},n}}{n_{br}} \tag{55}$$

where the material subscript r can represent air or HE products, n_{br} is the number of marker points of material r located in cell c , and θ_r is the volume fraction. The remaining variables of these particles are determined as those in the pure cell.

(3) In the interaction region which was inactive in the first two stages, particles are created to discretize the air and structure. After the conversion from FDM to MPM, the region is activated and discretized by material particles. Standard MPM described in Section 3.1 is employed to simulate the subsequent FSI . Compared with Eq.(30), the only difference is that the deviatoric stress has to be taken into account for the particles discretizing the structure and the stress is updated by

$$\sigma_{ijp}^{n+1} = \sigma_{ijp}^n + \Delta\Omega_{ijp}^n \sigma_{ijp}^n - \sigma_{ijp}^n \Delta\Omega_{ijp}^n + \Delta\sigma_{ijp}^n \tag{56}$$

where $\Delta\sigma_{ijp}^n$ is calculated by the material constitutive model introduced in Section 2.3.3.

3.4 Multi-material treating

The treatment of the moving interface is one of the key points in HE explosion simulation. In the process of detonation and fluid-structure interaction, the updated Lagrangian description is used and the interface can be exactly described by the particles. In the dispersion of HE products, the Eulerian description is used and the material particles degenerate to marker points which carry the position information for tracking the moving interface. The positions of the marker points are updated by the velocity field as described in Section 3.2.

As mentioned in Section 3.3, for mixed cells, a group of equations are solved to obtain the equilibration pressure at the cell-center points and the cell-center points carry the variables for different materials. Considering cell (i, j) in which both type of marker points are located, as shown in Fig.4. To calculate the volume fraction θ_1 of material 1 in the mixed cell (i, j) , we loop over all cells in time step $n - 1$. If a cell is a pure cell and is next to pure cells of other materials or mixed cells, it is deemed to be next to the material interface. The volume of this cell is distributed to the marker points within itself averagely as

$$V_m^{n-1} = \frac{V_c^{n-1}}{n_b^{n-1}} \tag{57}$$

where V_m^{n-1} is the volume carried by marker point m in the pure cell and n_b^{n-1} is the number of the marker points inside the pure cell. If a cell is a mixed cell, the volume of this cell is distributed to the marker points inside it by θ_r^{n-1} as

$$V_m^{r,n-1} = \frac{\theta_r^{n-1} V_c^{n-1}}{n_{br}^{n-1}} \quad r = 1, 2; \quad (58)$$

where $V_m^{r,n-1}$ is the volume carried by marker point m in the mixed cell and n_{br}^{n-1} is the number of marker points inside the mixed cell.

The volume fraction θ_r of material r in the mixed cell (i, j) in time step n can be obtained as

$$\theta_r^n = \frac{\sum_{m=1}^{n_{br}^n} V_m^{n-1}}{\sum_{m=1}^{n_{b1}^n} V_m^{n-1} + \sum_{m=1}^{n_{b2}^n} V_m^{n-1}} \quad (59)$$

With the determined volume fraction, the variables of the two materials in the mixed cell can be calculated based on two previously employed assumptions, i.e. the pressure of the two materials are equilibrated [Guilkey, Harman, and Banerjee (2007)] and the increment of specific internal energy is distributed to the two materials by volume fraction [Ning and Chen (2004)] as $e_r^{\text{int},n} = e_r^{\text{int},n-1} + \theta_r \Delta e_c^{\text{int}}$ where Δe_c^{int} is the specific internal energy increment in the cell-center point calculated by the governing equation. Thus, the relations between density $\rho_r (r = 1, 2)$, specific internal energy $e_r^{\text{int}} (r = 1, 2)$, volume fraction $\theta_r (r = 1, 2)$ and equilibration pressure p_e are

$$p_e = f_1(\rho_1, e_1^{\text{int}}) = f_2(\rho_2, e_2^{\text{int}}) \quad (60)$$

$$e_1^{\text{int}} = g_1(\rho_1, \theta_1) \quad (61)$$

$$e_2^{\text{int}} = g_2(\rho_2, \theta_2) \quad (62)$$

$$\theta_1 + \theta_2 = 1 \quad (63)$$

$$\rho_1 \theta_1 + \rho_2 \theta_2 = \rho_c \quad (64)$$

in which f_1 and f_2 are the EOS of the two materials and ρ_c is the density of the cell-center point obtained by mass conservation. The above equations can be solved together with Eq. (59) to obtain the six variables in cell (i, j) : ρ_1 , ρ_2 , e_1^{int} , e_2^{int} , θ_1 and θ_2 whilst the equilibration pressure p_e can be obtained by the EOS in Eq.(60). With the variables determined, the calculation in mixed cell (i, j) is completed.

Before proceeding to the numerical examples, the simulation is briefly summarized. Particles and marker points are employed to treat the moving interface in different stages and different ways. In detonation, HE and the surrounding air are discretized by particles and the interaction of the two materials at the interface is considered by the shape function of MPM. In the dispersion process, the HE products and surrounding air are discretized by the cells and the cell-center points. The particles degenerate to the marker points which only carry the position information. The marker points track the moving interface by updating their positions based on the velocity field. Furthermore, they are used to calculate the volume ratio between two materials in a mixed cell by carrying the volume information when they are in the cells next to material interface. In FSI, the marker points in pure cells are discarded and the regular particles are created according to the variables of cell-center points. The marker points in mixed cells are converted to particles again by retaining the position information and inheriting the conservation variables from the cell-center points as described in Section 3.3. The interfaces between HE products, air and the structure are tracked by the particles in MPM similar to that in the detonation discussed in Section 3.1.

4 Numerical examples

The afore-described scheme has been implemented in our MPM3D code to solve HE explosion problems. Five numerical examples are presented in this section to validate the scheme and demonstrate its capabilities.

4.1 One-dimensional TNT slab detonation

A 0.1 m long slab of TNT is detonated at the fixed left end as shown in Fig.6. The detonation wave travels to the right end at the detonation speed. This problem has been studied by using finite element method [Shin and Chisum (1997)] and SPH [Liu, Liu, Zong, and Lam (2003)] whose results can be used to validate the present code.

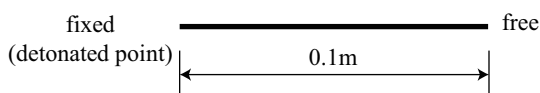


Figure 6: 1D TNT slab detonation

In this simulation, traditional MPM and the real detonation model with burn fraction specified in Section 2.3 are employed to simulate the process. The material parameters provided in Section 2.3 are adapted with 2000 particles initially located in

1000 cells. The pressure and density profiles along the TNT slab from $1\mu\text{s}$ to $14\mu\text{s}$ obtained by MPM3D are compared with the theoretical results [Zhang (1976)] and experimental results in Fig.7. The detonation peak pressures converge to between the experimental and theoretical CJ pressures whilst the detonation shock is well resolved.

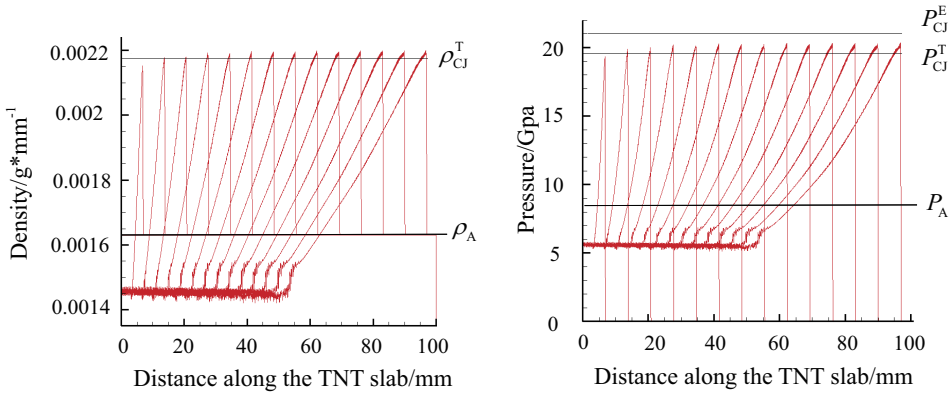


Figure 7: Profiles along the TNT slab in different moment during the detonation process (The superscripts E, T and A denote experimental, theoretical and artificial detonation model respectively)

Fig.7 also compares the results obtained by the artificial detonation model, see Section 2.3, and the real detonation model. In the former, which assumes infinite detonation speed, HE is considered initially as a group of gaseous products with the same energy, volume and density of the explosive charge. In the latter, the detonation along HE charge and the reaction rate are taken into account. Thus, the pressure jump which occurs when the shock front arrived at material interface is better captured in the real model than the artificial model. The similar observation is also noted in SPH [Liu and Liu (2003)].

4.2 One-dimensional Shock tube problem

Sod's shock tube problem [Sod (1978)] is often regarded as a standard test for simulation codes for compressible fluid. As shown in Fig. 8, this problem consists of a shock tube with a diaphragm separating two regions whose initial states are: $\rho_{\text{left}} = 1.0\text{g}/\text{mm}^3$, $p_{\text{left}} = 1.0\text{MPa}$, $\rho_{\text{right}} = 0.125\text{g}/\text{mm}^3$ and $p_{\text{right}} = 0.1\text{MPa}$. The fluids in both regions are initially at rest. At time $t = 0\text{ms}$, the diaphragm is ruptured. Then, the shock and the contact interface travel at different speeds. The results are

usually examined at $t = 0.143\text{ms}$ when the shock has travelled a distance of about 0.25mm . This problem is employed to test the capability of the FDM solver in AFDMP on simulating compressible fluid and does not involve conversion between FDM and MPM. The profiles of density, velocity and pressure are plotted in Fig.9 for a background mesh of 1000 cells. Good agreement with the analytical results can be seen. The simulation results obtained by MPM using the same background cells are also plotted in the figures and obvious numerical oscillations can be noted in the results. Unlike the MPM in which both the particles and background grid carry variables, the FDM solver in AFDMP method updates the variables only in the cell-center points and the marker points only carry position information. In this regard, the CPU times consumed by MPM and AFDMP are 78s and 46s, respectively. Furthermore, the convergence properties of AFDMP and MPM are studied by plotting the global error norms of the results against the changing of the background cell length (h), as shown in Fig. 10. The convergence rate of AFDMP is about 50% higher than that of MPM, which demonstrates the rationality of employing FDM to simulate the dispersion process in HE problems in AFDMP.

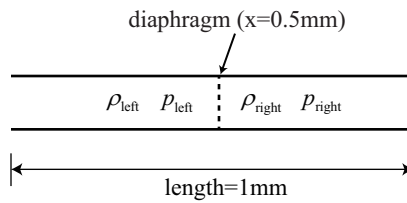


Figure 8: 1D shock tube problem

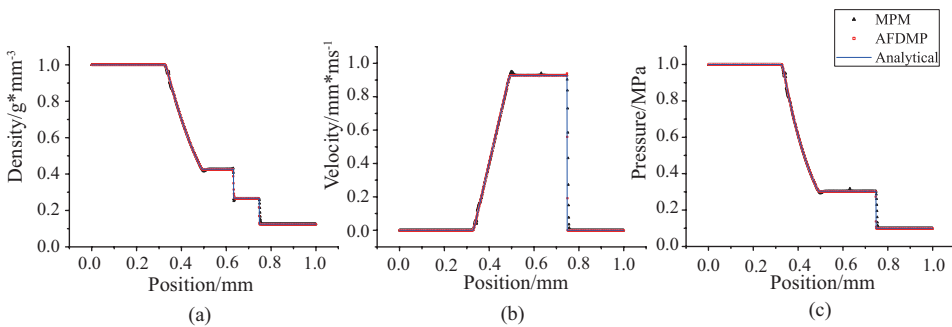


Figure 9: Profiles of density, velocity and pressure obtained by analytical solution, MPM and AFDMP

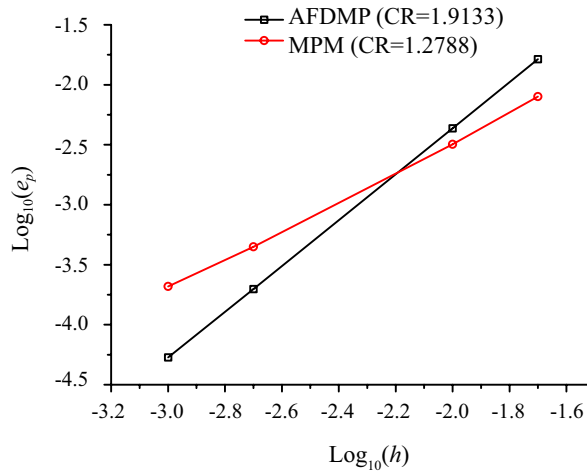


Figure 10: Error norms in pressure

4.3 Two-dimensional HE explosion produced gas dispersion

A two-dimensional HE explosion produced gas dispersion problem is simulated. The initial radius of the HE is 50 mm. The surrounding air is simulated by the air model in Section 2.3 and the boundary conditions are all “flow out”. This example is used to show the effectiveness of AFDMP for tracking the material interface and eliminating the non-physical penetration encountered by the standard MPM. The results obtained by the commercial software AUTODYN using the finite volume method are provided for reference. The 1000×1000 mm square computational domain is discretized by square cells of side length 1 mm in all the three methods. For AFDMP and MPM, 1 and 4 particles per background cell are used for air and TNT. Fig.11 and Fig.12 show respectively the colored contours of the material and pressure at $10\mu\text{s}$, $50\mu\text{s}$ and $90\mu\text{s}$. Near the material interface predicted by MPM, obvious non-physical penetration can be seen which also leads to non-physical oscillations of pressure. The results obtained by AFDMP and AUTODYN agree quite well with each other. On the other hand, the material interface obtained by AFDMP is smoother and more symmetric than that of AUTODYN because the interface tracking by the marker points is more accurate than the VOF method used in AUTODYN. As a result, the pressure contours obtained by AFDMP are better than those of AUTODYN in resolution. AFDMP and AUTODYN (FVM) consume similar amount of computational time and memory which are much less than those of MPM because the marker points in AFDMP carry less variables than the material particles.

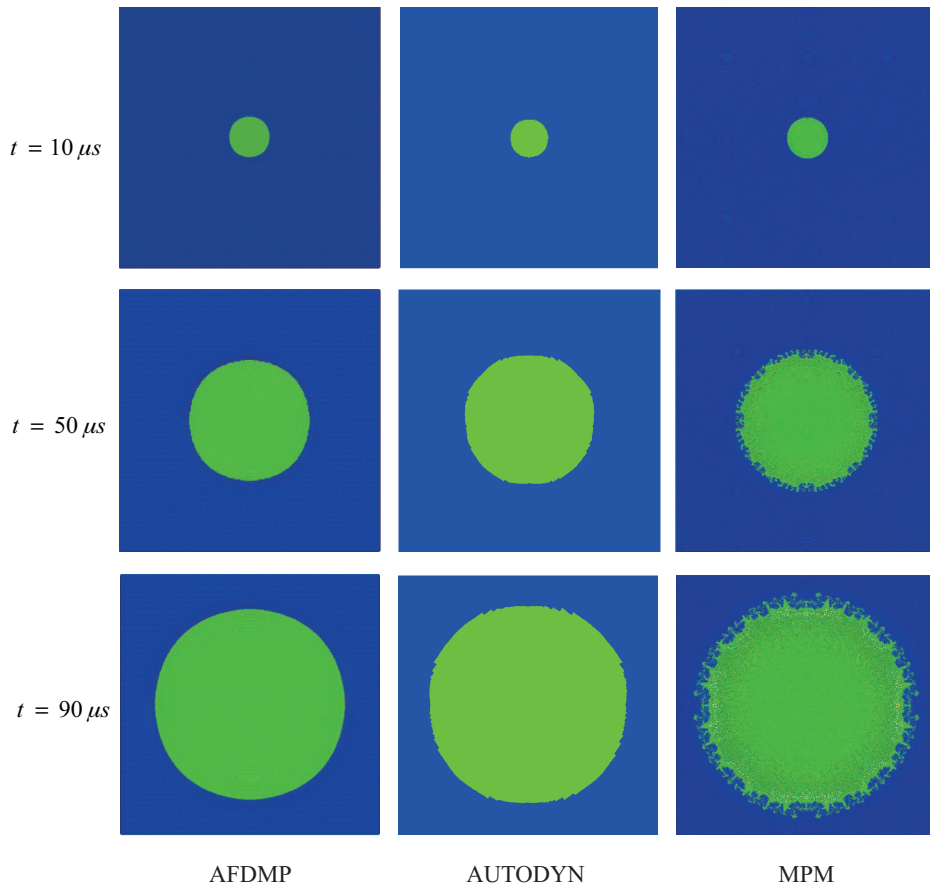


Figure 11: Contours of material at $t = 10\mu s$, $50\mu s$, $90\mu s$

4.4 Three-dimensional HE explosion produced gas dispersion

In this example, a three-dimensional HE explosion produced gas dispersion problem is simulated. A cube of TNT with side length 20 mm is detonated at its center. The surrounding air is driven by the gaseous products and the boundary conditions are all “flow out”. As introduced in Section 3, the detonation process is simulated by MPM and the dispersion process is simulated by FDM. The cubic computational domain of side length 500 mm is discretized by cubic background cells of side length 2.5 mm. For TNT and air, 8 and 1 particles per cell are employed, respectively. The colored contours of material and pressure in the dispersion process are plotted in Fig.13. It can be seen that the material interface is well-tracked and the symmetry is well-preserved. Fig.14 compares the overpressure peak along a

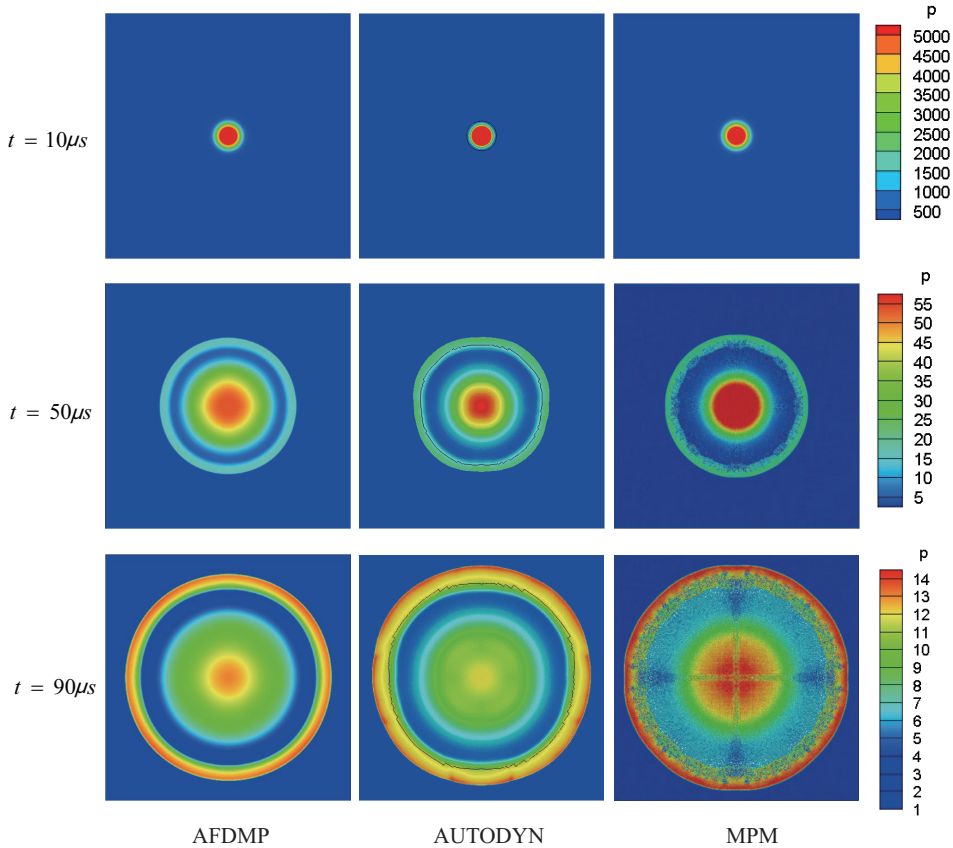


Figure 12: Contours of pressure at $t = 10\mu s$, $50\mu s$, $90\mu s$

radial line thru the center of the TNT. It shows that the results obtained by both AFDMP and AUTODYN are in good agreement with those of the empirical formula [Henrych (1979)] in far field, but are much lower in near field. This may be due to the grids are not fine enough to capture the sharp shock wave in near field. This suggests that a local refinement technique should be developed to enhance the accuracy in near field.

4.5 HE explosion produced gas dispersion and the interaction with the steel plate nearby

A two-dimensional problem similar to the one in Fig.1 is simulated by AFDMP. A circular disc of TNT is detonated at its center at $t = 0$. The gaseous products disperse to the surrounding air and finally the gas interact with a 20 mm-thick steel

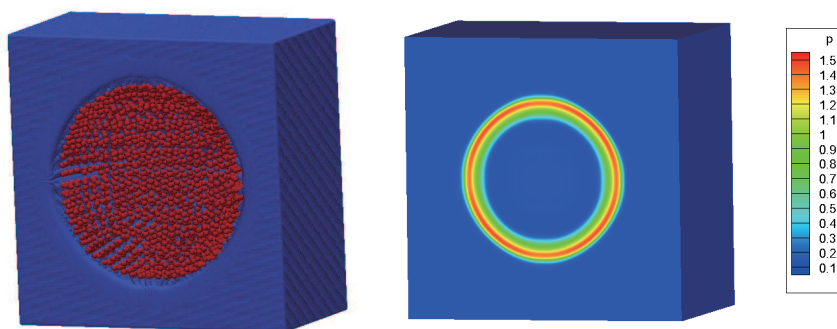


Figure 13: Colored contours of material and pressure

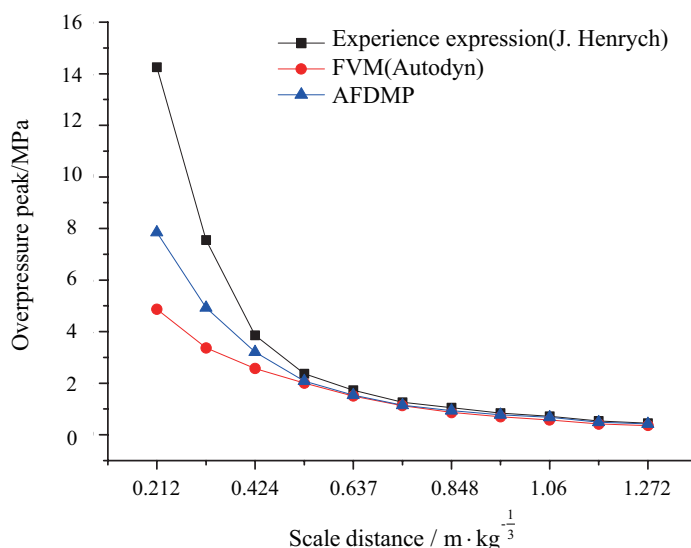


Figure 14: Overpressure peak along a radial line starting from the center of the TNT

plate 350 mm from the TNT. The boundary conditions are all “flow out”. The square computational region of side length 1000 mm is discretized into 1×1 mm background cells with 1 particle per cell for air and 4 particles per cell for both TNT and steel. The material models and parameters have been presented in Section 2.3. The colored contours of material and Mises stress in the steel plate at $t = 90\mu s$ are plotted in Fig.15 and 16, respectively. The results of AUTODYN are produced by using Eulerian-Lagrangian interaction method. The material interfaces obtained by

AFDMP is smoother and more symmetric than that of AUTODYN. On the other hand, the the Mises stress obtained by AFDMP agrees quite well with that of AUTODYN. The Mises stress time history of two points in the steel plate predicted by AFDMP and AUTODYN are shown in Fig.17. Again, reasonably good agreement can be noted.

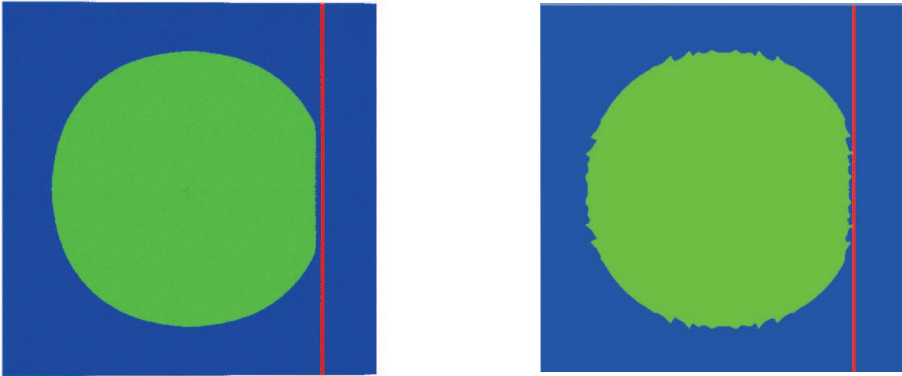


Figure 15: Contours of material at $t = 90\mu\text{s}$ (Left: AFDMP, Right: AUTODYN)

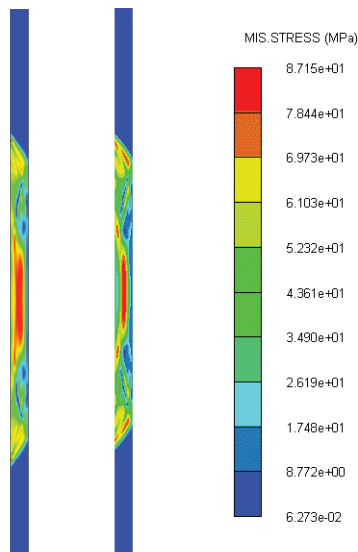


Figure 16: Contours of Mises stress in steel at $t = 90\mu\text{s}$ (Left: AFDMP, Right: AUTODYN)

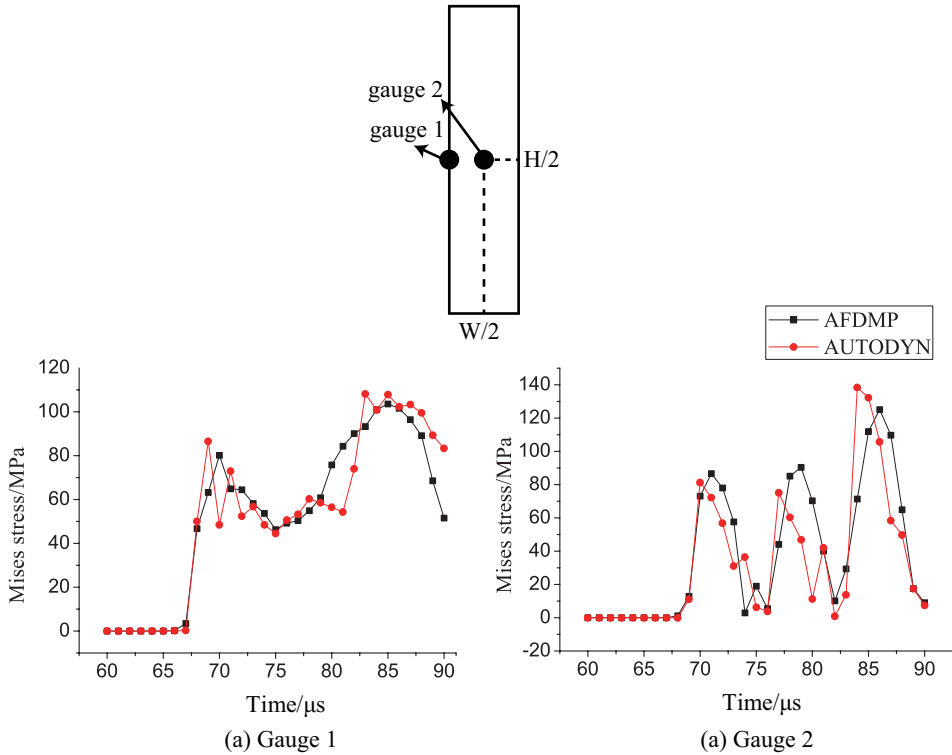


Figure 17: Time history of Mises stress in steel

5 Conclusion

A numerical scheme for simulating HE explosion and its effects on structures nearby has been proposed. It uses a Lagrangian frame description for the initiatory detonation and eventual FSI and, an Eulerian frame description for the dispersion of the detonation products to surrounding air. MPM is employed in Lagrangian frame description because of its ability for simulating history dependent materials and tracking the material interface in FSI with extreme deformation in the structure. FDM is employed in Eulerian frame description to avoid the non-physical penetration, which usually occurs in particle methods, at material interface between the detonation products and surrounding medium. During FDM stage, the material interface is tracked by the marker points which are degenerated from the particles in MPM and the mixed cell variables are determined based on two assumptions: the pressure of the two materials are equilibrating and the increment of specific internal energy is distributed to the two materials by volume fraction. The con-

version between MPM and FDM is implemented by the projection between the particles' variables in MPM and the cell centers' variables in FDM. The process involving history dependent materials and FSI is simulated by MPM whereas the process involving multi-material fluid problems is simulated by FDM. The conversion between MPM and FDM is launched based on a user-specified criteria. To conclude, the advantages of MPM and FDM are fully utilized in each stage of the HE explosion process.

Acknowledgement: Supported by the National Basic Research Program of China (2010CB832701), National Natural Science Foundation of China (11272180), Tsinghua University Initiative Scientific Research Program and Research Grant Council of Hong Kong (HKU 7173 09E).

References

- Aktay, L.; Johnson, A. F.** (2007): FEM/SPH coupling technique for high velocity impact simulations. *Advances in Meshfree Techniques*, pp. 147–167.
- Banerjee, B.** (2004): Material point method simulations of fragmenting cylinders. In *17th Engineering Mechanics Conference*.
- Benson, D. J.** (1992): Computational methods in Lagrangian and Eulerian hydrocodes. *Computer Methods in Applied Mechanics and Engineering*, vol. 99(2-3), pp. 235–394.
- Brackbill, J. U.; Ruppel, H. M.** (1986): Flip: a method for adaptively zoned, particle-in-cell calculations in two dimensions. *Journal of Computational Physics*, vol. 65, pp. 314–343.
- Fairlie, G.; Bergeron, D.** (2002): Numerical simulation of mine blast loading on structures. In *17th Military Aspects of Blast Symposium*.
- Gilmanov, A.; Acharya, S.** (2008): A hybrid immersed boundary and material point method for simulating 3d fluid-structure interaction problems. *International Journal for Numerical Methods in Engineering*, vol. 56, pp. 2151–2177.
- Guilkey, J.; Harman, T.; Banerjee, B.** (2007): An Eulerian Lagrangian approach for simulating explosions of energetic devices. *Computers and Structures*, vol. 85, pp. 660–674.
- Hallquist, J. O.** (1998): *LS-DYNA Theoretical Manual*. Livermore Software Technology Corporation.
- Han, Z. D.; Liu, H. T.; Rajendran, A. M.; Atluri, S. N.** (2006): The applications of Meshless Local Petrov-Galerkin (MLPG) approaches in high-speed

impact, penetration and perforation problems. *Computer Modeling in Engineering and Sciences*, vol. 14(2), pp. 119–128.

Henrych, J. (1979): *The dynamics of explosion and its use*. Elsevier Scientific Publishing Company.

Hu, W.; Chen, Z. (2006): Model-based simulation of the synergistic effects of blast and fragmentation on a concrete wall using the MPM. *International Journal of Impact Engineering*, vol. 32, pp. 2066–2096.

Jacinto, A. C.; Ambrosini, R. D.; Danesi, R. F. (2001): Experimental and computational analysis of plates under air blast loading. *International Journal of Impact Engineering*, vol. 25, pp. 927–947.

Johnson, G. R.; Cook, W. H. (1983): A constitutive model and data for metals subjected to large strains, high strain rates and high temperatures. In *7th International Symposium on Ballistics, The Hague, Netherlands: American Defense Preparedness Association*, pp. 541–547.

Lax, P. D.; Wendroff, B. (1964): Difference scheme for hyperbolic equations with high order of accuracy. *Communications on Pure and Applied Mathematics*, vol. 17, pp. 381–398.

Lian, Y. P.; Zhang, X.; Liu, Y. (2011): Coupling of finite element method with material point method by local multi-mesh contact method. *Computer Methods in Applied Mechanics and Engineering*, vol. 200, pp. 3482–3494.

Lian, Y. P.; Zhang, X.; Liu, Y. (2012): An adaptive finite element material point method and its application in extreme deformation problems. *Computer Methods in Applied Mechanics and Engineering*, vol. 241-244 (1), pp. 275–285.

Lian, Y. P.; Zhang, X.; Zhou, X.; Ma, S.; Zhao, Y. L. (2011): Numerical simulation of explosively driven metal by material point method. *International Journal of Impact Engineering*, vol. 38, pp. 238–246.

Liu, G. R.; Liu, M. B. (2003): *Smoothed particle hydrodynamics: a meshfree particle method*. World Scientific, Singapore.

Liu, M. B.; Liu, G. R.; Lam, K. Y.; Zong, Z. (2003): Meshfree particle simulation of the detonation process for high explosives in shaped charge unlined cavity configurations. *Shock Waves*, vol. 12(6), pp. 509–520.

Liu, M. B.; Liu, G. R.; Lam, K. Y.; Zong, Z. (2003): Smoothed particle hydrodynamics for numerical simulation of underwater explosion. *Computational Mechanics*, vol. 30, pp. 106–118.

Liu, M. B.; Liu, G. R.; Zong, Z.; Lam, K. Y. (2003): Computer simulation of high explosive explosion using smoothed particle hydrodynamics methodology. *Computers and Fluids*, vol. 32, pp. 305–322.

Liu, W. K.; Belytschko, T.; Chang, H. (1986): An arbitrary lagrangian-eulerian finite element method for path-dependent materials. *Computer Methods in Applied Mechanics and Engineering*, vol. 58, pp. 227–245.

Luccioni, B. M.; Ambrosini, R. D.; Danesi, R. F. (2004): Analysis of building collapse under blast loads. *Engineering Structures*, vol. 26, pp. 63–71.

Lucy, L. A. (1977): A numerical approach to the testing of the fission hypothesis. *Astrophysical Journal*, vol. 82, pp. 1013–1024.

Ma, J.; Hanan, J. C.; Komanduri, R.; Lu, H. (2012): Simulation of the deformation mechanisms of bulk metallic glass (BMG) foam using the material point method. *Computer Modeling in Engineering and Sciences*, vol. 86(4), pp. 349–382.

Ma, S.; Zhang, X.; Lian, Y. P.; Zhou, X. (2009): Simulation of high explosive explosion using adaptive material point method. *Computer Modeling in Engineering and Sciences*, vol. 39(2), pp. 101–123.

Ma, S.; Zhang, X.; Qiu, X. M. (2009): Comparison study of MPM and SPH in modeling hypervelocity impact problems. *International Journal of Impact Engineering*, vol. 36, pp. 272–282.

Ma, T. B.; Wang, C.; Ning, J. G. (2008): Multi-material Eulerian formulations and hydrocode for the simulation of explosions. *Computer Modeling in Engineering and Sciences*, vol. 33(2), pp. 155–178.

Ning, J. G.; Chen, L. W. (2004): Fuzzy interface treatment in eulerian method. *Science in China Series E-Engineering and Materials Science*, vol. 47(5), pp. 550–568.

Osher, S.; Fedkiw, R. P. (2001): Level set methods: an overview and some recent results. *Journal of Computational Physics*, vol. 169, pp. 463–502.

Shin, Y. S.; Chisum, J. E. (1997): Modeling and simulation of underwater shock problems using coupled lagrangian-eulerian analysis approach. *Shock and Vibration*, vol. 4(1), pp. 1–10.

Sod, G. A. (1978): A survey of several finite difference methods for systems of nonlinear hyperbolic conservation laws. *Journal of Computational Physics*, vol. 27, pp. 1–31.

Sulsky, D.; Chen, Z.; Schreyer, H. L. (1994): A particle method for history-dependent materials. *Computer Methods in Applied Mechanics and Engineering*, vol. 118(1-2), pp. 179–196.

Sulsky, D.; Zhou, S. J.; Schreyer, H. L. (1995): Application of a particle-in-cell method to solid mechanics. *Computer Physics Communications*, vol. 87(1-2), pp. 236–252.

Wu, C. Q.; Hao, H. (2005): Modeling of simultaneous ground shock and airblast pressure on nearby structures from surface explosions. *International Journal of Impact Engineering*, vol. 31, pp. 699–717.

Xu, K.; Lu, Y. (2006): Numerical simulation study of spallation in reinforced concrete plates subjected to blast loading. *Computers and Structures*, vol. 84, pp. 431–438.

Yanenko, N. N. (1971): *The method of fractional steps*. Springer-Verlag.

Youngs, D. L. (1982): Time dependent multi-material flow with large fluid distortion. *Numerical Methods for Fluid Dynamics*, pp. 273–285.

Zhang, D. L. (2010): *A course in computational fluid dynamics*. Higher Education Press.

Zhang, S. Z. (1976): *Detonation and its applications*. Beijing: Press of National Defense Industry.

Zhang, X.; Sze, K. Y.; Ma, S. (2006): An explicit material point finite element method for hyper-velocity impact. *International Journal for Numerical Methods in Engineering*, vol. 66, pp. 689–706.

Zhang, Y. J.; Xu, S. L. (2007): Numerical simulation on flow-structure interaction loaded by a blast wave from a central charge. *Journal of University of Science and Technology of China*, vol. 37, pp. 6–12.

Zukas, J.; Walters, W. (1998): *Explosive effects and applications*. Springer.